Letter

Hydrogenation Facilitates Proton Transfer through Two-Dimensional Honeycomb Crystals

Yexin Feng,[†,▽] Ji Chen,[‡,§,∥,▽] Wei Fang,[‡,§,⊥] En-Ge Wang,[#] Angelos Michaelides,*[,‡,§,∥] and Xin-Zheng Li*[,#]

[†]School of Physics and Electronics, Hunan University, Changsha 410082, P. R. China
[‡]Thomas Young Centre, University College London, London WC1E 6BT, United Kingdom
[§]London Centre for Nanotechnology, University College London, London WC1E 6BT, United Kingdom
[∥]Department of Physics and Astronomy, University College London, London WC1E 6BT, United Kingdom
[⊥]Department of Chemistry, University College London, London WC1E 6BT, United Kingdom
[#]School of Physics, ICQM, and Collaborative Innovation Center of Quantum Matter, Peking University, Beijing 100871, P. R. China

Ⓢ *Supporting Information*

ABSTRACT: Recent experiments have triggered a debate about the ability of protons to transfer easily through individual layers of graphene and hexagonal boron nitride (h-BN). However, state-of-the-art computer calculations have shown that the barriers to proton penetration can, at >3 eV, be excessively high. Despite considerable interest the origin of this apparent anomaly between experiment and simulation remains unclear. We offer a new perspective on this debate and show on the basis of first-principles calculations that the barrier for proton penetration is significantly reduced, to <1 eV, upon hydrogenation, even in the absence of pinholes in the lattice. Although hydrogenation has not been offered as an explanation before, analysis reveals that the barrier is reduced because hydrogenation destabilizes the initial state (a deep-lying chemisorption state) and expands the honeycomb lattice through which the protons penetrate. This study offers a rationalization of the fast proton transfer observed in experiments and highlights the ability of proton transport through single-layer materials in hydrogen-rich solutions.
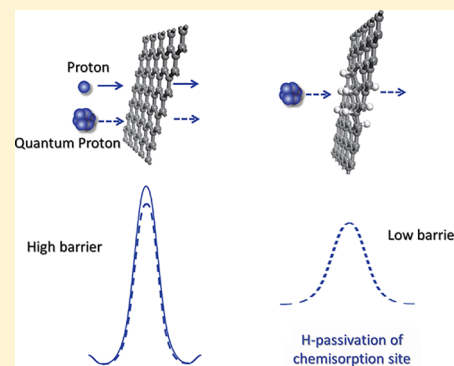
Selective sieving of ions and molecules through thin membranes is a key step for a wide range of applications such as water purification and ion exchange membrane fuel cells.[1−16] Two-dimensional (2D) materials like graphene and hexagonal boron nitride (h-BN) offer potential as membrane materials because they are a single atom thick and have high mechanical stability and flexibility.[1,2,4,5,7−10] For some time, it was believed that pristine graphene and h-BN were impermeable to ions due to high-energy barriers for penetration.[17,18] Recent experiments, however, have suggested that protons can, in fact, penetrate pristine graphene and h-BN.[1,2] In the measurements, the 2D materials were immersed in proton-conducting polymers or aqueous solutions, and from temperature (*T*)-dependent proton conductivity measurements, proton penetration barriers of only 0.8 and 0.3 eV were estimated for single-layer graphene and h-BN, respectively.[1] Note that these estimated barriers include contributions from zero-point energy (ZPE).[2] Defects such as atomic pinholes are known to facilitate proton transfer.[9] A certain level of defects will inevitably be present, associated, for example, with sp[3] carbon atoms.[19] However, in refs 1 and 2, various measurement techniques (transmission/tunnelling electron microscopy, Raman spectroscopy, and measurements

of gas leakage) were used to support the assertion that the proton-transfer mechanism was not facilitated by atomic defects in the membranes.

Considerable theoretical effort has been devoted toward understanding the microscopic details of how protons penetrate 2D materials.[9,17,18,20−22] It has been established on the basis of density functional theory (DFT) calculations that the barriers to proton penetration through pristine graphene and h-BN in vacuum can be excessively high. Specifically, computed barriers of 3.5 to 4.0 eV have been reported for chemisorbed protons (i.e., protons that are covalently bonded to the 2D materials) to penetrate graphene.[17,18,23] If the protons do not chemisorb on the surface but rather penetrate the sheet via a metastable physisorption state, smaller barriers of 1.4 to 2.6 eV have been reported.[17,18,23] However, the physisorption state is only a very shallow minimum, separated from the much more stable chemisorption state by a barrier of ≤0.1 eV.[24] Therefore, it seems unlikely that penetration from the physisorption state is the dominant mechanism for fast proton conduction.[22,24] When

an idealized theoretical model, in this case containing only pristine graphene and a proton, cannot rationalize the experimental observations, it is customary to question the quality of the calculations and to resort to more complex and more realistic models. Environmental effects such as the role of solvent and chemical decorations were therefore investigated.[22] Given the light mass of the proton, the role of nuclear quantum effects (NQEs) such as tunnelling and zero point motion could also be relevant, as shown, for example, through two interesting recent computational studies.[21,23] However, despite extensive effort,[9,17,18,20−22] no one was able to resolve the significant discrepancy between experiment and theory in understanding the dominant mechanism of facile proton transfer, and some even concluded that the problem may be beyond the scope of computational theory.[22]

We report a study of proton transfer through graphene and h-BN, focusing on the transmission mechanism. Consistent with previous studies, a very high potential energy barrier of ∼3.6 eV is found for proton penetration of graphene via the chemisorption state. Using ab initio path-integral molecular dynamics (PIMD),[25−31] we take into account NQEs and finite temperature thermal effects. We find that NQEs reduce the penetration barrier of graphene by 0.46 eV (12%) at 300 K, which is unlikely to be responsible for the experimentally observed high transfer rate. Upon considering the role sp^3-bonded atoms play on the penetration process, created here by hydrogenation of graphene and h-BN, we find that hydrogenation can reduce the penetration barriers significantly to <1 eV. This reduction arises because the hydrogenation induced sp^2 to sp^3 transformation destabilizes the deep-lying chemisorption state in which the proton can get trapped on the pristine membranes. Geometrically, hydrogenation also expands the six-atom rings through which protons transfer. Analysis of the penetration barriers associated with many distinct hydrogenated membranes reveals a clear correlation between the height of the penetration barriers and the local degree of hydrogenation at the proton-transfer site. Overall, this work highlights the significant difference in proton penetration barriers that can be found in the vicinities of sp^3-bonded atoms and helps to rationalize the facile transport of protons through single-layer materials.

Our DFT calculations were performed using the Vienna ab initio Simulation Package (VASP),[32] with an in-house implementation of the ab initio constrained-centroid molecular dynamics (MD) and PIMD methods.[28,33] The optB88-vdW functional was chosen in the electronic structure calculations so as to obtain a good description of the hydrogen (H)-bonding interactions and dispersion forces.[34,35] Charged cells were employed to describe the protons in the simulations, and we confirmed that any charge states considered were correctly characterized with Bader analysis.[36,37] We hydrogenated graphene to varying degrees without generating pinholes[38] using supercells ranging from 4 × 4 to 8 × 8. After hydrogenation, the supercell shape and size were allowed to change. For each partially hydrogenated structure, we have considered the two lowest energy structures following the study of ref 38. The climbing image nudged elastic band (cNEB) method was used in calculating the static penetration barriers,[39] with a force convergence criterion of 0.03 eV Å^{-1}, and all atoms were allowed to relax. Convergence of the reported barriers with respect to various computational setups including the size of the simulation cells was carefully tested, as detailed in the Supporting Information (SI).[40] Beyond the static description,

the classical and quantum free-energy profiles were obtained with constrained MD and PIMD approaches,[29−31] with the constraint applied on the vertical distance of the proton from the 2D layer. A 0.5 fs time step was used and the imaginary-time path in the PIMD simulations was sampled with 48 replicas, at a target temperature of 300 K. After thermalization, 30 000 steps (15 ps) were collected to calculate the constraint force for each constraint point. By integrating over the constraint forces, the free-energy profiles were obtained as detailed in the SI.[40]

On free-standing graphene protons adsorb preferentially at the chemisorption site directly above a carbon atom (Figure 1a). From the chemisorption site, our calculations yield a
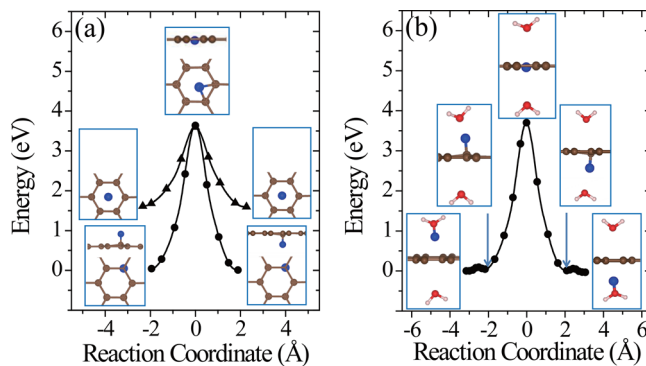
Figure 1. High barriers for proton transfer through pristine graphene. Calculated energy profiles as obtained from cNEB calculations for proton transfer across (a) pristine graphene and (b) graphene with adsorbed water molecules. Two energy profiles are shown in panel a, one between the metastable physisorption states (upper curve) and one between the chemisorption states (lower curve). The insets show some of the key states involved in the proton transfer processes. Brown (red, pink) balls are C (O, H) atoms. Protons are represented by blue balls.

proton penetration barrier of 3.60 eV. As noted, in previous experiments, the 2D layers were surrounded by proton-conducting polymers or aqueous solutions.[1,2,9,20,22] In the current study, we do not aim to model such an aqueous environment. However, to gain an initial understanding of how the presence of water might impact upon the proton penetration process, we employed the simplified model shown in the inset of Figure 1b. This model contains one water molecule on each side of the graphene layer, and with the addition of a proton it enables us to model proton transfer from an H_3O^+ on one side of the sheet to an H_2O on the other side of the sheet.[41] Our calculations show that the proton adsorbs at either the water molecule or the chemisorption site of the graphene sheet with very similar stability (Figure 1b). The metastable physisorption site for protons on free-standing graphene, as illustrated in Figure 1a, disappears due to the presence of water. The energy barrier for a proton to transfer from the H_3O^+ to the chemisorption site is <0.1 eV. The penetration barrier from the chemisorption site is 3.65 eV when water is present, very similar to the 3.60 eV obtained in the absence of water. The energy differences between physisorbed water molecules on different sites or with different orientations are only a few millielectronvolts,[41−43] so different configurations of water molecules will not obviously influence the energy profile of the proton penetration process.

Finite temperature and NQEs (ZPE and quantum tunneling) are known to alter the barriers of chemical processes,

particularly proton-transfer barriers. To understand the importance of such effects on the current system, we performed a series of ab initio MD and PIMD simulations from which free-energy barriers for proton penetration were obtained. The results of these simulations are shown in Figure 2. We find that
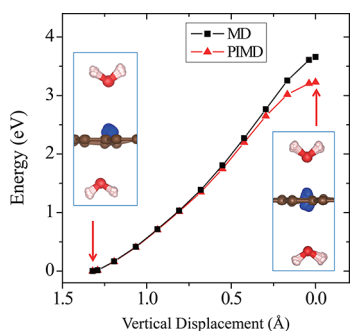
Figure 2. Free-energy profiles at 300 K obtained with ab initio constrained MD and PIMD simulations for proton transfer across a graphene sheet in the presence of water molecules. The MD simulations take into account thermal effects, whereas the PIMD simulations capture thermal and nuclear quantum effects. PIMD simulation snapshots for the initial state and transition state are also shown. Blue (red and pink) balls represent the beads of protons (O and H atoms) for one snapshot in a PIMD simulation. The centroids of the C atoms are shown as brown balls.

the pure thermal effects on the barrier are relatively small and the free-energy barrier in the model containing a water on either side of the sheet is 3.70 eV at 300 K. When NQEs are accounted for with PIMD the barrier is reduced by 0.46 eV at 300 K (Figure 2), quite a substantial reduction. Analysis reveals that this reduction in the free-energy barrier is due to enhanced quantum delocalization of the proton at the transition state compared with the initial state. This is similar behavior to that observed for H chemisorption on graphene[24] and is illustrated by the snapshots shown in Figure 2. The reduction arising from NQEs is also in line with that reported by Poltavsky et al. when similar PIMD methods are used,[23] although a different computational model and reaction pathway was considered by Poltavsky et al. However, considering the fact that the free-energy barrier for the process examined remains >3 eV at 300 K, we conclude that NQEs alone cannot rationalize the experimentally observed fast proton transfer.

We noted in the introduction that carbon atoms with sp^3 character are invariably present, even in pristine graphene.[19] The tiny barrier (91 meV) shown in Figure 1b for the proton to transfer from the (solvent) water molecule to the chemisorption state also indicates that hydrogenation of graphene is facile and that graphene sheets immersed in proton-conducting polymers or aqueous solutions could be hydrogenated or protonated to some extent. With this in mind we explored how the presence of chemisorbed hydrogens impacts the proton penetration barrier of graphene. Adsorbed hydrogens are examined because when they chemisorb they lead to an sp^2 to sp^3 hybridization of the carbon atoms they are bonded to but also because the hydrogenation of graphene is facile.[44] A broad range of hydrogenation scenarios was considered, ranging from having just a single chemisorbed hydrogen at a proton penetration site to fully hydrogenated graphene (graphane) sheets. Examples of some of the structures considered are shown in Figure 3, with full details given in the SI.[40] Upon computing the proton penetration barriers through the various
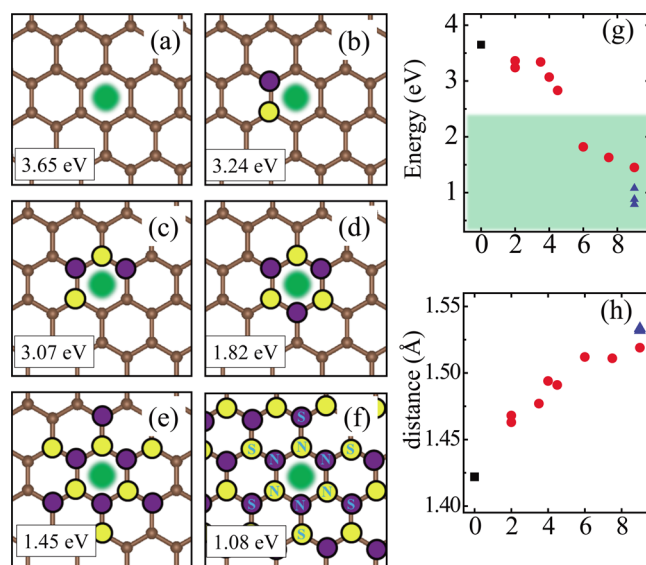
Figure 3. Hydrogenation facilitates proton penetration through graphene. (a–f) Atomic structures of graphene and a selection of hydrogenated graphene sheets with different degrees of local hydrogenation. cNEB energy barriers for proton transfer through each sheet are also reported. Yellow and violet dots indicate C atoms hydrogenated from the top and bottom sides, respectively. The large smeared green ball indicates the hole of the C ring through which the proton penetrates. In panel f the nearest-neighbor (N) and second-nearest-neighbor (S) C atoms to the penetration site are indicated. (g) cNEB barriers as a function of the degree of local hydrogenation (D_{local}^H) for various hydrogenated structures. (See Figures S4 and S5 for details of the structures.) The green shaded area indicates low penetration barriers with high D_{local}^H. (h) Averaged C–C bond distance of the six-C ring through which the proton penetrates as a function of D_{local}^H. In panels g and h, the black square and red dots represent data for proton transfer across pristine and partially hydrogenated graphene, respectively. The three blue triangles in panels g and h indicate data for the chair, boat, and disordered configurations of the fully hydrogenated graphene. In panel h, three blue triangles are close to each other, all with values of ~1.53 Å.

hydrogenated and partially hydrogenated sheets considered, we find that hydrogenation leads to reduced proton penetration barriers. The actual barriers obtained depend sensitively on the particular hydrogenation structure, with barriers for some hydrogenated structures reduced very substantially to <1 eV.

Let us now look more closely at the hydrogenated systems and try to understand the barriers obtained. Crucially we find that the penetration of protons through a single atom layer is a local process and that the height of the penetration barrier depends primarily on the local degree of hydrogenation in the vicinity of the penetration site. To show this more clearly, we introduce an order parameter, D_{local}^H. D_{local}^H is defined as $D_{local}^H = N_N^H + w \times N_S^H$, with N_N^H (N_S^H) being the number of hydrogenated atoms at the nearest (second-nearest) neighbors of the hole (indicated by N and S in the Figure 3f) and w representing a weight factor capturing the importance of hydrogenation at the second-nearest sites. The barriers as a function of D_{local}^H, with w set to 0.5, are plotted in Figure 3g (tuning w from 0.2 to 0.8 gives similar results (Figure S11)). Upon computing D_{local}^H for all barriers considered, we found two interesting features: (i) a clear correlation exists between the penetration barrier and D_{local}^H, with the barrier getting smaller as D_{local}^H increases, and (ii) the systems can be categorized into two main groups, with the most significant barrier reduction being

found for $D_{local}^H > 6$. Systems with D_{local}^H smaller than 6 belong to the group with large barriers. In these systems, the six-C ring through which the proton penetrates is not fully hydrogenated. C atoms with sp^2 bonding are present in the ring, and the proton can chemisorb at these sites before penetration (Figures S4 and S5). It is the presence of the very stable chemisorption sites that lead to particularly high barriers for proton penetration. For the systems considered, when $D_{local}^H \geq 6$, the ring is fully hydrogenated. The sp^3 bonding eliminates the deep-lying chemisorption state before penetration. In so doing the initial state energy is raised and the barriers are <2.0 eV. Note that this analysis reveals that because the barrier is related to the local extent of hydrogenation a sample does not need to have a very high global degree of hydrogenation for low barrier proton penetration sites to exist. All that is required is a high local degree of hydrogenation, and indeed surface science measurements and previous calculations show that upon hydrogenation there is a tendency for H atoms to cluster.[38,45,46]

Aside from eliminating the chemisorption well, sp^3-bonded carbons also lead to an expansion of the lattice. This can be seen in Figure 3h, where the averaged C−C distance of a hexagon is shown to increase with D_{local}^H. This expansion is an additional geometric effect played by sp^3-bonded carbons.[47]

Our simulations with full hydrogenation correspond to the case when the graphene layer is fully hydrogenated around a local penetration site. They have the same D_{local}^H but different barriers in Figure 3g (three blue triangles). To understand why this happens, we take the chair conformation and a disordered H configuration as examples and show the actual cNEB barrier profiles in Figure 4. The key difference between these two
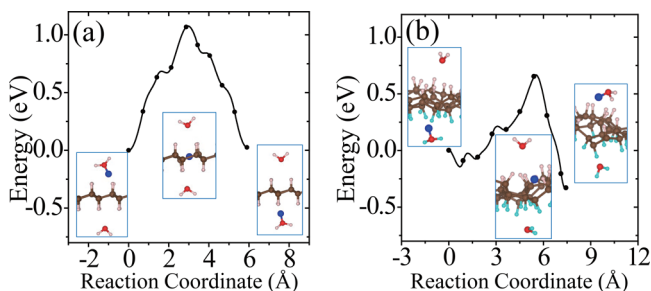
Figure 4. Energy profiles for proton transfer across fully hydrogenated graphene with (a) the chair conformation and (b) a disordered H configuration. Insets show the atomic structures for the initial, transition, and final states. Red (pink, brown) balls are O (H, C) atoms. Protons are represented by blue balls. For the disordered conformation, the H adatoms below the sheets are colored with cyan (a contrast to pink) for clarity. The specific disordered and asymmetric decoration pattern reported in panel b yields a particularly low proton penetration barrier. Additional information on these structures is given in Figure S13.

systems is that in the chair conformation the upper and lower sides of the graphene sheet are similarly hydrogenated, while in the disordered configuration the two sides of the sheet are hydrogenated to different extents. Such asymmetric decoration creates structures wherein it is yet more facile for the proton to penetrate form one side to the other. On a larger scale, one can imagine that hydrogenation can induce different local penetration sites, with the ease of penetration related to the extent of hydrogenation on either side of the sheet. Besides this, motivated by the loop-structure promoted proton transfer in the formation of ammonium bisulfate on water surface,[48] we

also investigated other proton penetration mechanisms involving proton exchange on partially and fully hydrogenated graphene (Figures S17 and S18). The cNEB barriers are comparable to those of the direct proton penetration processes. The penetration happens directly from the physisorption sites, and the structures of the transition states are similar to those in the direct proton penetration processes (Figures S17 and S18). Therefore, hydrogenation-induced destabilization of chemisorption sites is still the main reason for the low proton penetration barriers.

For h-BN, H atoms also prefer to chemisorb in pairs on B and N atoms, and the averaged binding energy between H atoms and h-BN increases with the degree of hydrogenation.[49,50] As with graphene, upon examining proton penetration through h-BN we find that the barriers decrease upon hydrogenation. As shown in Table 1, the barrier through

Table 1. Calculated cNEB Barrier, ZPE Corrections (ΔE_{ZPE}) and Corrected Barrier (Barrier) for Proton Transfer Across Pristine and Hydrogenated Graphene and h-BN Sheets[a]

	cNEB Barrier	ΔE_{ZPE}	barrier
$G_{pristine}$	3.65	−0.26	3.39
$G_{chair-H}$	1.08	−0.07	1.06
G_{boat-H}	0.88	−0.12	0.76
$G_{disordered-H}$	0.79	−0.18	**0.61**
h-BN$_{pristine}$	3.33	−0.21	3.12
h-BN$_{stirrup-H}$	1.43	−0.53	0.90
h-BN$_{boat-H}$	1.91	−0.35	1.56
h-BN$_{disordered-H}$	0.93	−0.39	**0.51**

[a]The rightmost column should be compared with the experimental values of 0.8 and 0.3 eV in ref 1. ΔE_{ZPE} is estimated as the ZPE differences between the initial and transition states. $G_{pristine}$ and h-BN$_{pristine}$ are pristine graphene and h-BN sheets. $G_{chair-H}$, G_{boat-H}, $G_{disordered-H}$, h-BN$_{stirrup-H}$, h-BN$_{boat-H}$, and h-BN$_{disordered-H}$ are hydrogenated 2D sheets with various H conformations. Water molecules are present on either side of the sheet for all systems reported here. The lowest barrier for each material is indicated in bold.

pristine h-BN is as high as 3.33 eV. In fully hydrogenated h-BN with ordered H configurations (h-BN sheets with stirrup and boat conformations, h-BN$_{stirrup-H}$ and h-BN$_{boat-H}$),[51] the barrier can be reduced to <2.0 eV. For disordered H configurations, the barrier further decreases to ∼0.93 eV. Some representative energy profiles for partially and fully hydrogenated h-BN sheets are provided in the Figures S14−S16.

In Table 1, we summarize some representative barriers obtained for proton transfer through the various graphene and h-BN systems considered. Also included in Table 1 are the ZPE corrections to the barriers computed within the harmonic approximation. ZPE effects decrease the barriers to proton penetration in all systems considered, and when they are taken into consideration the lowest barrier on graphene is 0.61 eV and on h-BN it is 0.51 eV. Finally, we note that we have also considered how substitution of proton for deuteron is likely to alter the penetration barriers. Treating this again at the ZPE level we find a 50 meV difference in penetration barriers between proton and deuteron for $G_{disordered-H}$ and a 120 meV difference between proton and deuteron for h-BN$_{disordered-H}$. In each case, the deuteron barrier is slightly larger than the proton barrier, in agreement with recent computational work[21] and experiment.[2]

To conclude, we have reported a theoretical study on proton transfer through graphene and h-BN. After considering in detail

various factors that could impact on the penetration barriers for protons, we find that sp^3 hybridization at the penetration site, achieved here through hydrogenation, plays a key role in reducing these barriers to <1.0 eV. Although hydrogenation has not been suggested before as a means to facile proton transfer, the physical origin of barrier reduction hydrogenation facilitates is remarkably straightforward. It arises simply because the deep-lying chemisorption states are destabilized and the honeycomb lattice at the penetration site expands. Combining the major influence from hydrogenation and minor influence from NQEs, the experimentally observed low-proton-transfer barrier can be rationalized. Considering the fact that 2D materials can be functionalized with various elements other than H, for example, O, OH, F, and Cl, this study suggests that there could be further scope for more controllable ion and proton sieving. We hope that this analysis on the atomistic details of facile proton transfer can stimulate further theoretical, experimental, and application oriented studies toward the design of improved 2D membrane materials and devices.

ASSOCIATED CONTENT

Ⓢ Supporting Information

The Supporting Information is available free of charge on the ACS Publications website at DOI: 10.1021/acs.jpclett.7b02820.

> Computational details of DFT calculations and PIMD simulations; tests of the computational setup; calculated cNEB barriers for proton penetration with various functionals; more atomic structures of hydrogenated graphene and h-BN sheets; the zoom-in view of the asymmetric H decoration on hydrogenated graphene and h-BN with disordered H conformations; the mean constraint forces as a function of PIMD beads; the classical and quantum free-energy profiles for proton transfer across single-layer pristine h-BN sheet; and discussion of the isotope effects and ZPE corrections. (PDF)

AUTHOR INFORMATION

Corresponding Authors

*A.M.: E-mail: angelos.michaelides@ucl.ac.uk.
*X.-Z.L.: E-mail: xzli@pku.edu.cn.

ORCID Ⓞ

Yexin Feng: 0000-0001-5925-8645
Ji Chen: 0000-0003-1603-1963
Angelos Michaelides: 0000-0002-9169-169X
Xin-Zheng Li: 0000-0003-0316-4257

Author Contributions

▽Y.F. and J.C. contributed equally to this work.

Notes

The authors declare no competing financial interest.

ACKNOWLEDGMENTS

REFERENCES

(1) Hu, S.; Lozada-Hidalgo, M.; Wang, F.; Mishchenko, A.; Schedin, F.; Nair, R.; Hill, E.; Boukhvalov, D.; Kat-snelson, M.; Dryfe, R.; et al. Proton transport through one-atom-thick crystals. *Nature* **2014**, *516*, 227.

(2) Lozada-Hidalgo, M.; Hu, S.; Marshall, O.; Mishchenko, A.; Grigorenko, A.; Dryfe, R.; Radha, B.; Grigorieva, I.; Geim, A. Sieving hydrogen isotopes through two-dimensional crystals. *Science* **2016**, *351*, 68.

(3) Abraham, J.; Vasu, K. S.; Williams, C. D.; Gopinadhan, K.; Su, Y.; Cherian, C. T.; Dix, J.; Prestat, E.; Haigh, S. J.; Grigorieva, I. V.; et al. Tunable sieving of ions using graphene oxide membranes. *Nat. Nanotechnol.* **2017**, *12*, 546.

(4) Surwade, S. P.; Smirnov, S. N.; Vlassiouk, I. V.; Unocic, R. R.; Veith, G. M.; Dai, S.; Mahurin, S. M. Water desalination using nanoporous single-layer graphene. *Nat. Nanotechnol.* **2015**, *10*, 459.

(5) Cohen-Tanugi, D.; Grossman, J. C. Mechanical strength of nanoporous graphene as a desalination membrane. *Nano Lett.* **2012**, *12*, 3602.

(6) Zilman, A.; Pearson, J.; Bel, G. Effects of jamming on nonequilibrium transport times in nanochannels. *Phys. Rev. Lett.* **2009**, *103*, 128103.

(7) O'Hern, S. C.; Stewart, C. A.; Boutilier, M. S. H.; Idrobo, J. C.; Bhaviripudi, S.; Das, S. K.; Kong, J.; Laoui, T.; Atieh, M.; Karnik, R. Selective molecular transport through intrinsic defects in a single layer of CVD graphene. *ACS Nano* **2012**, *6*, 10130.

(8) Celebi, K.; Buchheim, J.; Wyss, R. M.; Droudian, A.; Gasser, P.; Shorubalko, I.; Kye, J. I.; Lee, C.; Park, H. G. Ultimate permeation across atomically thin porous graphene. *Science* **2014**, *344*, 289.

(9) Achtyl, J. L.; Unocic, R. R.; Xu, L.; Cai, Y.; Raju, M.; Zhang, W.; Sacci, R. L.; Vlassiouk, I. V.; Fulvio, P. F.; Ganesh, P.; et al. Aqueous proton transfer across single-layer graphene. *Nat. Commun.* **2015**, *6*, 6539.

(10) O'Hern, S. C.; Boutilier, M. S. H.; Idrobo, J. C.; Song, Y.; Kong, J.; Laoui, T.; Atieh, M.; Karnik, R. Selective ionic transport through tunable subnanometer pores in single-layer graphene membranes. *Nano Lett.* **2014**, *14*, 1234.

(11) Joshi, R.; Carbone, P.; Wang, F.; Kravets, V.; Su, Y.; Grigorieva, I.; Wu, H.; Geim, A.; Nair, R. Precise and ultrafast molecular sieving through graphene oxide membranes. *Science* **2014**, *343*, 752.

(12) Mi, B. Graphene oxide membranes for ionic and molecular sieving. *Science* **2014**, *343*, 740.

(13) Kim, H. W.; Yoon, H. W.; Yoon, S. M.; Yoo, B. M.; Ahn, B. K.; Cho, Y. H.; Shin, H. J.; Yang, H.; Paik, U.; Kwon, S.; et al. Selective Gas Transport through Few-Layered Graphene and Graphene Oxide Membraned. *Science* **2013**, *342*, 91.

(14) Li, H.; Francisco, J. S.; Zeng, X. C. Unraveling the mechanism of selective ion transport in hydrophobic subnanometer channels. *Proc. Natl. Acad. Sci. U. S. A.* **2015**, *112*, 10851.

(15) Cheng, C.; Jiang, G.; Garvey, C. J.; Wang, Y.; Simon, G. P.; Liu, J. Z.; Li, D. Ion transport in complex layered graphene-based membranes with tuneable interlayer spacing. *Sci. Adv.* **2016**, *2*, e1501272.

(16) Secchi, E.; Marbach, S.; Niguès, A.; Stein, D.; Siria, A.; Bocquet, L. Massive radius-dependent flow slippage in carbon nanotubes. *Nature* **2016**, *537*, 210.

(17) Miao, M.; Nardelli, M. B.; Wang, Q.; Liu, Y. First principles study of the permeability of graphene to hydrogen atoms. *Phys. Chem. Chem. Phys.* **2013**, *15*, 16132.

(18) Wang, W. L.; Kaxiras, E. Graphene hydrate: theoretical prediction of a new insulating form of graphene. *New J. Phys.* **2010**, *12*, 125012.

(19) Ni, Z. H.; Ponomarenko, l. A.; Nair, R. R.; Yang, R.; Anissimova, S.; Grigorieva, I. V.; Schedin, F.; Blake, P.; Shen, Z. X.; Hill, E. H.; et al. On resonant scatterers as a factor limiting carrier mobility in graphene. *Nano Lett.* **2010**, *10*, 3868.

(20) Walker, M. I.; Braeuninger-Weimer, P.; Weatherup, R. S.; Hofmann, S.; Keyser, U. F. Measuring the proton selectivity of graphene membranes. *Appl. Phys. Lett.* **2015**, *107*, 213104.

(21) Zhang, Q.; Ju, M.; Chen, L.; Zeng, X. C. Differential permeability of proton isotopes through graphene and graphene analogue monolayer. *J. Phys. Chem. Lett.* **2016**, *7*, 3395.

(22) Kroes, J. M. H.; Fasolino, A.; Katsnelson, M. I. Density functional based simulations of proton permeation of graphene and hexagonal boron nitride. *Phys. Chem. Chem. Phys.* **2017**, *19*, 5813.

(23) Poltavsky, I.; Zheng, L.; Mortazavi, M.; Tkatchenko, A. Quantum tunneling of thermal protons through pristine graphene. 2016, arXiv:1605.06341v1 [physics.chem-ph]. arXiv.org e-Print archive. http://128.84.21.199/abs/1605.06341v1.

(24) Davidson, E. R. M.; Klimeš, J.; Alfè, D.; Michaelides, A. Cooperative interplay of van der Waals forces and quantum nuclear effects on adsorption: H at graphene and at coronene. *ACS Nano* **2014**, *8*, 9905.

(25) Marx, D.; Parrinello, M. Ab initio path-integral molecular dynamics. *Z. Phys. B: Condens. Matter* **1994**, *95*, 143.

(26) Tuckerman, M. E.; Marx, D.; Klein, M. L.; Parrinello, M. Efficient and general algorithms for path integral CarCParrinello molecular dynamics. *J. Chem. Phys.* **1996**, *104*, 5579.

(27) Tuckerman, M. E.; Marx, D.; Klein, M. L.; Parrinello, M. On the quantum nature of the shared proton in hydrogen bonds. *Science* **1997**, *275*, 817.

(28) Guo, J.; Lu, J. T.; Feng, Y.; Chen, J.; Peng, J.; Lin, Z.; Meng, X.; Wang, Z.; Li, X. Z.; Wang, E. G.; et al. Nuclear quantum effects of hydrogen bonds probed by tip-enhanced inelastic electron tunneling. *Science* **2016**, *352*, 321.

(29) Tuckerman, M. E.; Marx, D. Heavy-atom skeleton quantization and proton tunneling in "intermediate-barrier" hydrogen bonds. *Phys. Rev. Lett.* **2001**, *86*, 4946.

(30) Zhang, Q.; Wahnström, G.; Björketun, M.; Gao, S.; Wang, E. Path Integral Treatment of Proton Transport Processes in BaZrO3. *Phys. Rev. Lett.* **2008**, *101*, 215902.

(31) Walker, B.; Michaelides, A. Direct assessment of quantum nuclear effects on hydrogen bond strength by constrained-centroid ab initio path integral molecular dynamics. *J. Chem. Phys.* **2010**, *133*, 174306.

(32) Kresse, G.; Furthmüller, J. Efficiency of ab-initio total energy calculations for metals and semiconductors using a plane-wave basis set. *Comput. Mater. Sci.* **1996**, *6*, 15.

(33) Chen, J.; Li, X. Z.; Zhang, Q. F.; Probert, M. I. J.; Pickard, C. J.; Needs, R. J.; Michaelides, A.; Wang, E. G. Quantum simulation of low-temperature metallic liquid hydrogen. *Nat. Commun.* **2013**, *4*, 2064.

(34) Klimeš, J.; Bowler, D. R.; Michaelides, A. Chemical accuracy for the van der Waals density functional. *J. Phys.: Condens. Matter* **2010**, *22*, 022201.

(35) Klimeš, J.; Bowler, D. R.; Michaelides, A. Van der Waals density functionals applied to solids. *Phys. Rev. B: Condens. Matter Mater. Phys.* **2011**, *83*, 195131.

(36) Bader, R. *Atoms in Molecules: A Quantum Theory*; Oxford University Press: New York, 1990.

(37) Henkelman, G.; Arnaldsson, A.; Jónsson, H. A fast and robust algorithm for Bader decomposition of charge density. *Comput. Mater. Sci.* **2006**, *36*, 354.

(38) Šljivančanin, Z.; Andersen, M.; Hornekær, L.; Hammer, B. Structure and stability of small H clusters on graphene. *Phys. Rev. B: Condens. Matter Mater. Phys.* **2011**, *83*, 205426.

(39) Henkelman, G.; Uberuaga, B. P.; Jónsson, H. A climbing image nudged elastic band method for finding saddle points and minimum energy paths. *J. Chem. Phys.* **2000**, *113*, 9901.

(40) See the Supporting Information for details of the method and computational setups.

(41) Kurita, T.; Okada, S.; Oshiyama, A. Energetics of ice nanotubes and their encapsulation in carbon nanotubes from density-functional theory. *Phys. Rev. B: Condens. Matter Mater. Phys.* **2007**, *75*, 205424.

(42) Ma, J.; Michaelides, A.; Alfè, D.; Schimka, L.; Kresse, G.; Wang, E. Adsorption and diffusion of water on graphene from first principles. *Phys. Rev. B: Condens. Matter Mater. Phys.* **2011**, *84*, 033402.

(43) Hamada, T. Adsorption of water on graphene: A van der Waals density functional study. *Phys. Rev. B: Condens. Matter Mater. Phys.* **2012**, *86*, 195436.

(44) Lin, C. F.; Feng, Y. X.; Xiao, Y. D.; Durr, M.; Huang, X. Q.; Xu, X. Z.; Zhao, R. G.; Wang, E. G.; Li, X. Z.; Hu, Z. H. Direct observation of ordered configurations of hydrogen adatoms on graphene. *Nano Lett.* **2015**, *15*, 903.

(45) Hornekær, L.; Rauls, E.; Xu, W.; Šljivančanin, Z.; Otero, R.; Stensgaard, I.; Lægsgaard, E.; Hammer, B.; Besenbacher, F. Clustering of chemisorbed H (D) atoms on the graphite (0001) surface due to preferential sticking. *Phys. Rev. Lett.* **2006**, *97*, 186102.

(46) Guisinger, N. P.; Rutter, G. M.; Crain, J. N.; First, P. N.; Stroscio, J. A. Exposure of epitaxial graphene on SiC (0001) to atomic hydrogen. *Nano Lett.* **2009**, *9*, 1462.

(47) Leenaerts, O.; Peelaers, H.; Hernández-Nieves, A. D.; Partoens, B.; Peeters, F. M. First-principles investigation of graphene fluoride and graphane. *Phys. Rev. B: Condens. Matter Mater. Phys.* **2010**, *82*, 195436.

(48) Li, L.; Kumar, M.; Zhu, C.; Zhong, J.; Francisco, J. S.; Zeng, X. C. Near-barrierless ammonium bisulfate formation via a loop-structure promoted proton-transfer mechanism on the surface of water. *J. Am. Chem. Soc.* **2016**, *138*, 1816.

(49) Kroes, J. M. H.; Fasolino, A.; Katsnelson, M. I. Density functional based simulations of proton permeation of graphene and hexagonal boron nitride. *Phys. Chem. Chem. Phys.* **2016**, *18*, 19359.

(50) Khvostov, V. V.; Konyashin, I. Y.; Shouleshov, E. N.; Babaev, V. G.; Guseva, M. B. Surface modification of boron nitride in hydrogen plasma. *Appl. Surf. Sci.* **2000**, *157*, 178.

(51) Samarakoon, D. K.; Wang, X. Q. Intrinsic half-metallicity in hydrogenated boron-nitride nanoribbons. *Appl. Phys. Lett.* **2012**, *100*, 103107.